THE ASTROPHYSICAL JOURNAL, 365:261–268, 1990 December 10


# VLA OBSERVATIONS OF HIGH-VELOCITY H I ASSOCIATED WITH THE HERBIG-HARO OBJECTS 7–11

L. F. RODRÍGUEZ[1,2], S. LIZANO,[1,3] J. CANTÓ,[1] V. ESCALANTE,[1,2] AND I. F. MIRABEL[4]

*Received 1990 February 2; accepted 1990 June 12*

## ABSTRACT

We report VLA observations of the 21 cm hyperfine transition of H I and of the adjacent continuum toward the HH 7–11 region. At the velocity of the cloud we detect two H I emission zones that are associated with SVS 3 and BD +30°549, the young stars that illuminate the reflection nebula NGC 1333. We suggest that these are photodissociated H I regions.

At intermediate velocities ($\pm 20$ km s$^{-1}$ with respect to the radial velocity of the ambient cloud) we detect H I bipolar outflows associated with HH 7–11 and HH 12. The H I outflow morphologies are similar to those observed previously in CO, although we better resolve the second bipolar outflow (the one associated with HH 12). None of the proposed exciting sources of the HH 12 outflow is located at the centroid of the bipolar H I outflow. The HH objects 7–11 and 12 appear projected along the edge of their respective blueshifted H I lobes. This result may imply that these HH objects are not necessarily jetlike phenomena but instead trace the walls of the cavity produced by the stellar wind. In the 20 km s$^{-1}$ blueshifted channel we also detect several other sites of intermediate-velocity emission whose origin is uncertain but that may signal additional outflow sites, of monopolar geometry, in the cloud. At higher velocities ($\pm 40$ km s$^{-1}$ with respect to the radial velocity of the ambient cloud), we can still detect the high-velocity bipolar H I emission associated with HH 7–11. The +40 km s$^{-1}$ H I emission lobe is more compact than the +20 km s$^{-1}$ H I emission lobe, as expected for a decelerating outflow. We conclude that the H I mapped with the VLA is the decelerated, lower velocity extension of the extremely high-velocity atomic gas detected by Lizano *et al.* with Arecibo.

*Subject headings:* nebulae: individual (NGC 1333)—nebulae: internal motions — nebulae: reflection — radio sources: 21 cm radiation — stars: pre–main-sequence.

## I. INTRODUCTION

Energetic mass outflows are known to be present in the early stages of stellar evolution. Perhaps the best-studied manifestation of mass outflow in young stars are the bipolar molecular outflows. A major puzzle regarding bipolar outflows has been the identification of their driving agent. Since the discovery of the phenomenon in 1980 it has been generally assumed that the high-velocity (tens of km s$^{-1}$) molecular gas observed in the bipolar outflows had been accelerated by a much faster (hundreds of km s$^{-1}$), but more tenuous stellar wind. However, direct observational evidence for such fast and powerful winds was missing.

An important development in this problem was the detection in HH 7–11 of extremely high-velocity gas, both in atomic (H I) and molecular (CO) form (Lizano *et al.* 1988). This extremely high-velocity gas spreads over $\sim 350$ km s$^{-1}$ and its momentum rate is sufficient to drive the CO bipolar outflow known to exist in the region (Edwards and Snell 1983). The H I observations of Lizano *et al.* (1988) were made at Arecibo with a modest angular resolution of $\sim 3'$, and no conclusions could be reached regarding the geometry of the extremely high-velocity H I. In this paper we present VLA observations of H I associated with HH 7–11 and its environment. The observations reveal interesting components of atomic hydrogen both at the cloud velocity and at high velocities and suggest that H I observations of regions of active star formation are, at least in the case of HH 7–11, a very important tool to understand the different phenomena present.

## II. OBSERVATIONS

The 21 cm hyperfine transition of H I ($\nu = 1420.406$ MHz) and the adjacent continuum were observed in 1988 July 8 and 15 with the Very Large Array of the NRAO.[5] The VLA was then in the D configuration, providing an angular resolution of 53″ (for natural weight maps) at 21 cm. All our observations were made having as phase center the position of SVS 13 [$\alpha(1950) = 03^h25^m58^s.2$; $\delta(1950) = 31°05'46''$], the object believed to be the exciting source of the HH 7–11 system (Strom, Vrba, and Strom 1976; Cohen and Schwartz 1983; Grossman *et al.* 1987; Sandell *et al.* 1990). The amplitude calibrator was 3C 286, with an adopted 21 cm flux of 14.7 Jy. The phase calibrator was 0333+321, for which a bootstrapped flux of $3.2 \pm 0.1$ Jy was determined. We also observed 0538+498 as bandpass calibrator, but there was absorption from line-of-sight H I, and we could not perform a reliable bandpass calibration. This limitation did not affect significantly the quality of the data since we were using relatively narrow bandwidths (6.25 MHz). During the July 8 run we used one IF with 64 channels of 97.7 kHz (for a velocity resolution of 20.6 km s$^{-1}$), and during the July 15 run we used two IFs, each with 32 channels of 195.3 kHz (for a velocity resolution of 41.2 km s$^{-1}$). The first data set provides higher velocity resolution that the second, and with it we had as primary goal the study of H I components of intermediate velocity ($\sim 20$ km s$^{-1}$). The

[1] Instituto de Astronomía, UNAM.
[2] Harvard-Smithsonian Center for Astrophysics.
[3] Osservatorio Astrofisico di Arcetri.
[4] Centre d'Etudes Nucléaires de Saclay.

[5] The National Radio Astronomy Observatory is operated by Associated Universities Inc., under cooperative agreement with the National Science Foundation.

second data set provides better signal-to-noise ratio with lower velocity resolution and was obtained to study broader H I components, such as those observed by Lizano *et al.* (1988). In both cases we centered the spectrometer at 8.0 km $s^{-1}$, the radial LSR velocity of the ambient cloud. Also in both cases the central 75% of the total bandwidth was recorded in a continuum channel. The data were edited and calibrated following the standard VLA procedures.

## III. OBSERVATIONAL RESULTS

### *a) Continuum*

We concatenated all the data bases for the continuum channel to produce a continuum map as sensitive as possible. In Figure 1 we show a natural-weight, CLEANed map of the region. We detected 58 sources above the level of 5 $\sigma$, which was 0.60 mJy for the center of the field. The positions and fluxes of these sources are given in Table 1. From the results of Condon (1984) and the formulation of Rodríguez *et al.* (1989*b*), we estimate that the expected number of background sources at 1.4 GHz within one primary VLA beam is given by

$$\langle N \rangle \simeq 38 S_0^{-0.7} , \quad (1)$$

where $S_0$ is the detectable flux density threshold at the center of the field given in mJy. For $S_0 = 0.6$ mJy, we obtain $\langle N \rangle = 54 \pm 7$. From this estimate we can conclude that most of the sources detected are background objects. We note, however, that they appear to be more numerous on the west half of our map than on the east half. Source 44 in Table 1 has been discussed previously (Rodríguez and Cantó 1983; Snell and Bally 1986) and found to have a nonthermal spectrum (flux decreasing with frequency). These authors conclude that this source most probably is an extragalactic object.

There are, nevertheless, several radio continuum sources that are almost certainly related with the HH 7–11 region.

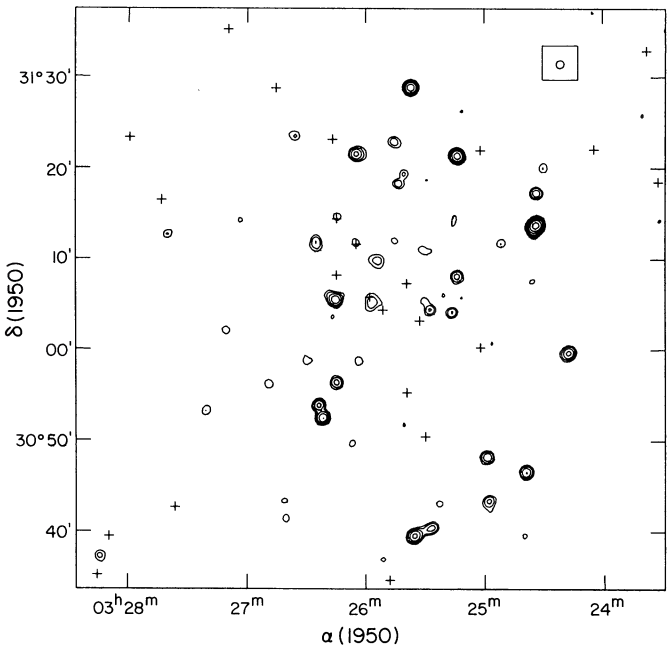


FIG. 1.—Natural-weight, CLEANed map of the 21 cm continuum from the HH 7–11 region. Contours are 5, 10, 20, 40, 80, 160, and 360 times 1 $\sigma$, which was 0.12 mJy. The half power contour of the beam (53″ × 53″) is also shown. This map and those in the following figures are not corrected for the primary beam response, and the sources away from the phase center appear with fluxes smaller than real. The positions of the *IRAS* sources in the region are marked with crosses.

TABLE 1

21 CENTIMETER CONTINUUM SOURCES IN HH 7–11 REGION

| Number | α(1950) | δ(1950) | $S_\nu$[a] (mJy) |
|---|---|---|---|
| 1..... | 3h23m31s.4 | 31°14′21″ | 11.6 |
| 2..... | 3 23 40.1 | 31 25 48 | 52.9 |
| 3..... | 3 24 05.1 | 31 37 02 | 46.4 |
| 4..... | 3 24 17.8 | 30 59 41 | 23.9 |
| 5..... | 3 24 30.1 | 31 20 05 | 9.3 |
| 6..... | 3 24 33.7 | 31 17 19 | 14.2 |
| 7..... | 3 24 33.9 | 31 13 49 | 159.1 |
| 8..... | 3 24 35.7 | 31 07 37 | 4.7 |
| 9..... | 3 24 39.3 | 30 46 36 | 29.4 |
| 10..... | 3 24 40.2 | 30 39 37 | 22.7 |
| 11..... | 3 24 51.3 | 30 11 49 | 2.4 |
| 12..... | 3 24 56.2 | 31 00 44 | 1.1 |
| 13..... | 3 24 57.9 | 30 43 25 | 26.0 |
| 14..... | 3 24 58.7 | 30 48 16 | 17.6 |
| 15..... | 3 25 11.4 | 31 26 19 | 2.8 |
| 16..... | 3 25 11.6 | 31 05 48 | 1.0 |
| 17..... | 3 25 13.5 | 31 21 23 | 36.5 |
| 18..... | 3 25 13.8 | 31 08 09 | 5.0 |
| 19..... | 3 25 15.0 | 31 14 31 | 3.6 |
| 20..... | 3 25 16.4 | 31 04 09 | 3.2 |
| 21..... | 3 25 20.6 | 31 06 04 | 1.2 |
| 22..... | 3 25 22.8 | 30 43 08 | 4.6 |
| 23..... | 3 25 26.9 | 30 40 27 | 26.1 |
| 24..... | 3 25 27.4 | 31 04 26 | 3.5 |
| 25..... | 3 25 29.0 | 31 18 42 | 1.9 |
| 26..... | 3 25 29.9 | 31 05 23 | 1.2 |
| 27..... | 3 25 31.0 | 31 11 03 | 1.3 |
| 28..... | 3 25 35.4 | 30 39 36 | 93.6 |
| 29..... | 3 25 37.1 | 31 28 53 | 72.8 |
| 30..... | 3 25 40.6 | 31 19 25 | 2.5 |
| 31..... | 3 25 40.7 | 30 51 49 | 1.3 |
| 32..... | 3 25 43.4 | 31 18 22 | 3.3 |
| 33..... | 3 25 45.2 | 31 12 05 | 1.0 |
| 34..... | 3 25 45.6 | 31 22 56 | 7.1 |
| 35..... | 3 25 51.3 | 30 37 01 | 7.3 |
| 36..... | 3 25 53.8 | 31 09 54 | 4.3 |
| 37..... | 3 25 56.7 | 31 05 17 | 3.0 |
| 38..... | 3 26 03.5 | 30 58 50 | 1.2 |
| 39..... | 3 26 04.8 | 31 21 35 | 12.8 |
| 40..... | 3 26 04.8 | 31 11 51 | 1.3[b] |
| 41..... | 3 26 06.8 | 30 49 47 | 1.9 |
| 42..... | 3 26 14.4 | 31 14 45 | 1.8 |
| 43..... | 3 26 14.8 | 30 56 28 | 5.4 |
| 44..... | 3 26 15.2 | 31 05 34 | 11.4 |
| 45..... | 3 26 16.8 | 31 03 40 | 0.7 |
| 46..... | 3 26 21.7 | 30 52 34 | 16.7 |
| 47..... | 3 26 23.8 | 30 53 56 | 9.4 |
| 48..... | 3 26 25.1 | 31 11 53 | 3.6 |
| 49..... | 3 26 30.1 | 30 58 49 | 3.0 |
| 50..... | 3 26 35.8 | 31 23 33 | 7.2 |
| 51..... | 3 26 40.4 | 30 41 30 | 6.5 |
| 52..... | 3 26 41.1 | 30 43 24 | 3.9 |
| 53..... | 3 26 49.0 | 30 56 15 | 2.6 |
| 54..... | 3 27 03.5 | 31 14 19 | 1.6 |
| 55..... | 3 27 10.8 | 31 02 08 | 4.6 |
| 56..... | 3 27 20.6 | 30 53 19 | 4.5 |
| 57..... | 3 27 40.2 | 31 12 45 | 5.3 |
| 58..... | 3 28 13.9 | 30 37 18 | 142.9 |

[a] Flux density corrected for primary beam response.

[b] Flux density approximately corrected for line contamination.

Sources 37, 40, and 42 in Table 1 are associated with *IRAS* point sources, (see Fig. 1), and with the objects $H_2O$(B), SVS 3, and BD +30°549 (Haschick *et al.* 1980; Strom, Vrba and Strom 1976; Harvey, Wilking, and Joy 1984). Sources 37 and 40 correspond to sources 4 and 3, respectively, in Snell and Bally (1986). The 1.4 GHz fluxes determined by us for these sources (3.0 and 1.3 mJy) are similar to those found at 4.9 GHz (2.0 and 1.0 mJy; Snell and Bally 1986; Haschick *et al.* 1980). It should be noted that the continuum flux of source 40 given in Table 1 has been approximately corrected for contamination by line emission since the continuum map was made from a channel that includes both continuum and line. This line contamination resulted (see below) in an increase of ~0.6 mJy in the apparent continuum emission. No problems of this type are expected in the other continuum sources, since line emission is in general weak. As we see below, on the basis of their association with high-velocity blueshifted H I, it appears likely that a few other radio continuum sources could be embedded in the HH 7–11 cloud.

We finally note that the radio continuum emission observed in association with SVS 3 and BD +30°549 exceeds that expected from free-free emission from a photoionized, optically thin H II region. This is a well-known problem in star formation that has been discussed recently by Natta *et al.* (1988), Curiel *et al.* (1989), and Rodríguez *et al.* (1989*b*), among others. For example, SVS 3 has a bolometric luminosity of 360 $L_\odot$ (Harvey *et al.* 1984), which corresponds to a B5 ZAMS star with an ionizing flux of $1.7 \times 10^{42}$ s$^{-1}$ (Thompson 1984). At a distance of 350 pc this ionizing flux will produce an H II region with a flux density of ~0.15 mJy in the optically thin regime, below the value of 1.0 mJy found at 4.9 GHz by Snell and Bally (1986).

*b*) H I *Line Emission at the Velocity of Ambient Cloud*

We will discuss now the data with a velocity resolution of 20.6 km s$^{-1}$. We made natural-weight maps and subtracted the continuum using an average map made with the channels from −486 to −177 km s$^{-1}$ and 173 to 482 km s$^{-1}$, regions where no line emission is expected. There was significant line emission (or absorption) only in the three central channels, at −12.6, 8.0, and 28.6 km s$^{-1}$. In Figure 2 we show the maps for these channels together with a continuum map included for comparison purposes.

The 8 km s$^{-1}$ map (tracing mainly gas from the ambient cloud) shows three regions with significant signal, one in absorption and two in emission. The feature in absorption coincides with the position of the continuum source 7, the brightest in our field (see Table 1), and we interpret it as simply due to line-of-sight absorption by gas from the ambient cloud. An average (over the 20.6 km s$^{-1}$ width of the channel) optical depth of ~0.4 is obtained. This continuum source is most probably a background extragalactic source since it is rela-

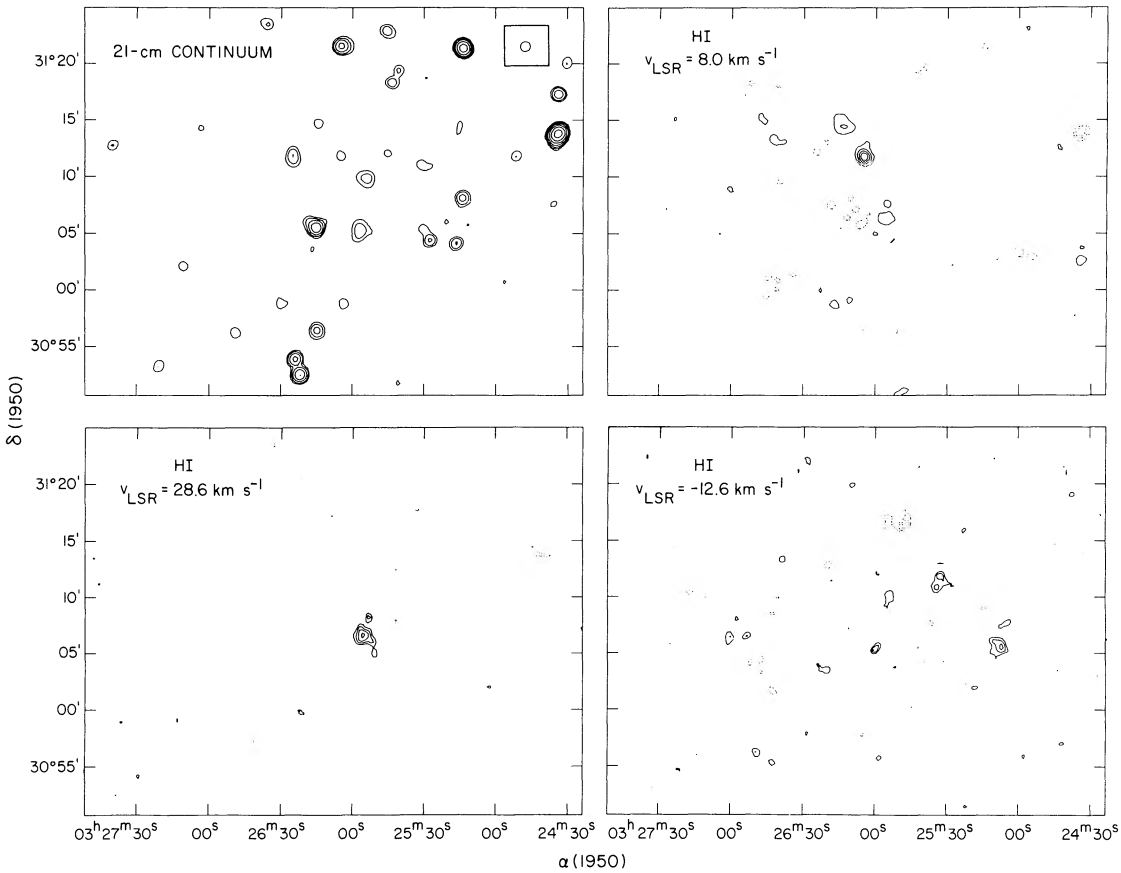


FIG. 2.—Natural-weight VLA maps of the HH 7–11 region. *Top left*: Continuum at 21 cm. *Top right*: H I map for $v_{LSR}$ = 8.0 km s$^{-1}$, the ambient cloud radial velocity. *Bottom left*: H I map for $v_{LSR}$ = 28.6 km s$^{-1}$, tracing redshifted gas. *Bottom right*: H I map for $v_{LSR}$ = −12.6 km s$^{-1}$, tracing blueshifted gas. Contours of the continuum map are as in Fig. 1. Contours for the $v_{LSR}$ = 8.0 km s$^{-1}$ map are −20, −15, −10, −5, 5, 10, 15, and 20 mJy beam$^{-1}$. Contours for the velocity-shifted maps are −6, −5, −4, −3, 3, 4, 5, and 6 mJy beam$^{-1}$. The half-power contour of the beam is shown in the continuum map. The positions and fluxes (corrected for primary beam response) of the sources in the H I maps are given in Table 2.

TABLE 2

H I COMPONENTS IN HH 7–11 REGION

| Number | $\alpha$(1950) | $\delta$(1950) | $S_\nu$[a] (mJy) | Comments |
|---|---|---|---|---|
| Gas at Cloud Velocity ($v_{LSR}$ = 8.0 km s$^{-1}$) | | | | |
| 1..... | 3$^h$24$^m$34$^s$.0 | 31°13′49″ | −56.2 | Absorption against background source |
| 2..... | 3 25 56.6 | 31 06 24 | 8.0 | Red lobe of HH 7–11 outflow |
| 3..... | 3 26 04.9 | 31 11 48 | 29.5 | SVS 3 |
| 4..... | 3 26 13.5 | 31 14 30 | 13.6 | BD +30°549 |
| Redshifted Gas ($v_{LSR}$ = 28.6 km s$^{-1}$) | | | | |
| 1..... | 3$^h$25$^m$53$^s$.2 | 31°08′14″ | 4.5 | Red lobe of HH 12 outflow |
| 2..... | 3 25 55.9 | 31 06 46 | 6.3 | Red lobe of HH 7–11 outflow |
| Blueshifted Gas ($v_{LSR}$ = −12.6 km s$^{-1}$) | | | | |
| 1..... | 3$^h$25$^m$06$^s$.9 | 31°05′34″ | 7.6 | |
| 2..... | 3 25 32.6 | 31 11 53 | 5.9 | Associated with radio continuum |
| 3..... | 3 25 34.0 | 31 10 55 | 5.1 | Associated with radio continuum |
| 4..... | 3 25 47.8 | 31 16 22 | −7.6 | |
| 5..... | 3 25 53.8 | 31 10 04 | 4.1 | Blue lobe of HH 12 outflow |
| 6..... | 3 26 00.5 | 31 05 16 | 5.3 | Blue lobe of HH 7–11 outflow |
| 7..... | 3 26 19.8 | 31 03 30 | 4.0 | |
| 8..... | 3 26 49.1 | 30 56 13 | 7.4 | Associated with radio continuum |
| 9..... | 3 26 53.3 | 31 06 32 | 6.2 | |
| 10..... | 3 27 00.3 | 31 06 27 | 6.7 | |

[a] Peak flux density corrected for primary beam response.

tively bright in the radio and does not have an *IRAS* counterpart. The two H I emission zones detected by us are associated with *IRAS* sources and with the radio continuum sources 40 and 42, as well as with the stars BD +30°549 and SVS 3 (see Table 2). In Figure 3 we show the H I emission associated with SVS 3 and BD +30°549, superposed on a gray-scale plot of the red POSS plate. These two stars illuminate NGC 1333, the reflection nebula to the northeast of HH 7–11.

The average brightness temperature of a line source is given by

$$\left(\frac{T_B}{\mathrm{K}}\right) = 870\left(\frac{S_\nu}{\mathrm{mJy}}\right)\left(\frac{\lambda}{21\ \mathrm{cm}}\right)^2\left(\frac{\theta_S}{\mathrm{arcsec}}\right)^{-2}\left(\frac{\Delta v_i}{\Delta v_l}\right), \quad (2)$$

where $S_\nu$ is the flux density of the line, $\lambda$ is the observing frequency, $\theta_S$ is the angular diameter of the source, $\Delta v_i$ is the instrumental resolution in velocity (channel width), and $\Delta v_l$ is the line width. Since the H I emission regions do not appear resolved spatially for our angular resolution of 53″ or in velocity for our velocity resolution of 20.6 km s$^{-1}$, we obtain lower limits for the brightness temperature of 4 K (for the source associated with BD +30°549) and 9 K (for the source associated with SVS 3). We can also estimate the H I mass from

$$\left(\frac{M_{\mathrm{H\,I}}}{M_\odot}\right) = 2.3 \times 10^{-4}\left(\frac{S_\nu}{\mathrm{mJy}}\right)\left(\frac{\Delta v_i}{\mathrm{km\ s^{-1}}}\right)\left(\frac{D}{\mathrm{kpc}}\right)^2, \quad (3)$$

where $D$ is the distance of the source, and we have assumed optically thin H I emission. For $\Delta v_i = 20.6$ km s$^{-1}$ and $D = 350$ pc (Herbig and Jones 1983) we derive values for the H I mass of 0.008 $M_\odot$ (for the BD +30°549 component) and 0.017 $M_\odot$ (for the SVS 3 component). If the H I line emission were optically thick, these values would be lower limits.

We can think of two explanations for the H I emission regions: (1) they are regions where the H I has higher brightness temperature than the average value (this making them detectable by contrast in an interferometer map) or (2) they are regions where a certain amount of $H_2$ has been dissociated into H I. The first explanation seems unlikely on the following arguments. As shown in the Appendix, the H I emission most probably is optically thin. The intensity of optically thin H I emission does not depend on the excitation temperature of the gas, so, for a given column density of gas, hotter H I will give the same intensity as cooler H I. It then appears plausible to conclude that we are observing photodissociated regions, most probably by the UV radiation of SVS 3 and BD +30°549. Envelopes of atomic hydrogen, most probably tracing photodissociated regions, have been previously observed around some young stars (e.g., Read 1980; Dewdney and Roger 1986). In the Appendix we present an interpretation for these H I emission regions in terms of photodissociation. We finally note that, at a marginal level, there is also H I emission associated with the red lobe of the HH 7–11 outflow (see Table 2).

### c) H I *Line Emission at* ±20.6 km s$^{-1}$

We turn now our attention to the velocity-shifted channels. The map from the blueshifted ($v_{LSR}$ = −12.6 km s$^{-1}$) channel shows two regions of emission that correspond well with the blueshifted components seen by Edwards and Snell (1983) in association with HH 7–11 and HH 12 (see Figs. 2 and 4). The map from the redshifted ($v_{LSR}$ = 28.6 km s$^{-1}$) channel shows that the single lobe seen by Edwards and Snell (1983) in between HH 7–11 and HH 12 clearly breaks into two components (see Fig. 4). These results imply that two distinct bipolar outflows are present, a hypothesis that was considered by Edwards and Snell (1983) but that could not be decided from their data. The map of Liseau, Sandell, and Knee (1988) also shows the redshifted lobes of HH 7–11 and HH 12 as a single structure. We note also that if the blueshifted and redshifted lobes near HH 12 are powered by a single object located between the lobes, neither SVS 11 or SVS 12 (see Fig. 4) have the required position. Another object that has been proposed as the exciting source of HH 12 is the T Tauri star 107 of

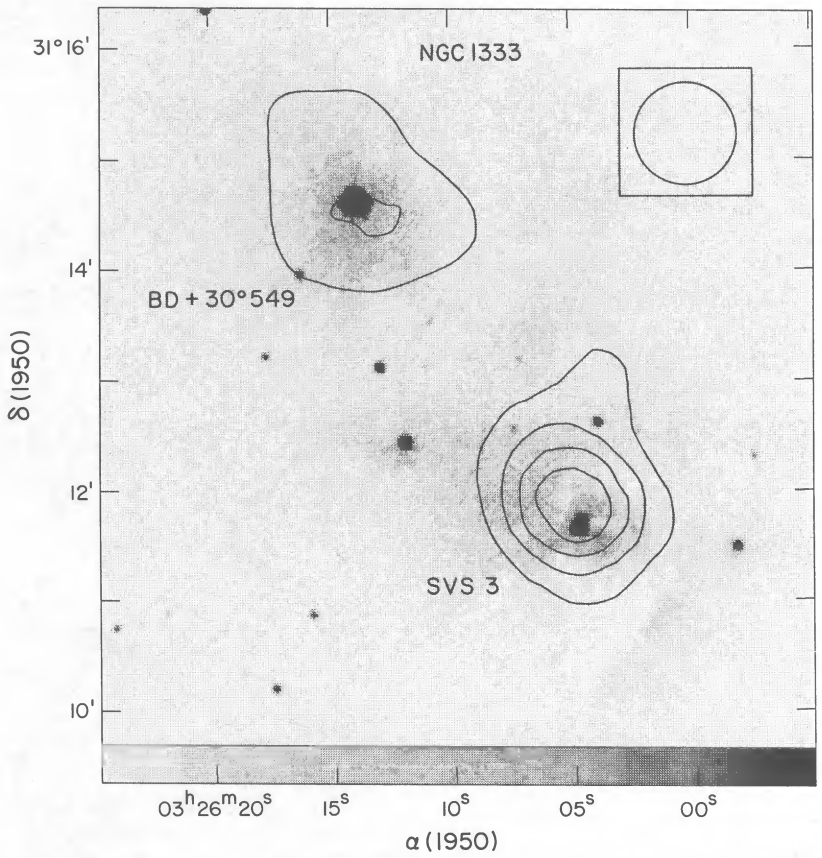


FIG. 3.—H I emission at $v_{LSR} = 8.0$ km s$^{-1}$ superposed on a gray-scale representation of the HH 7–11 region from the digitized Red POSS images of Klinglesmith and Hollis (1987). The H I emission zones are approximately centered on BD +30°549 and SVS 3, the illuminating stars of the reflection nebula NGC 1333. Contours are 5, 10, 15, and 20 mJy beam$^{-1}$.

Strom, Strom, and Stocke (1983), located at $\alpha(1950) = 03^h25^m52^s.5$; $\delta(1950) = 31°07'46''.0$, but this object is not at the centroid of the outflow. An alternative explanation is that the blueshifted lobe is powered by SVS 12, while the redshifted lobe is powered by SVS 11 (see Fig. 4), but the proper motions of HH 12 (roughly directed to the north; see Herbig and Jones 1983) seem to rule out this explanation. We also note that there are no detected radio continuum (see Fig. 1 and Table 1), or *IRAS* sources (Jennings *et al.* 1987) at the centroid of the HH 12 bipolar outflow. Finally, there is no strong $NH_3$ emission at that position (Ho and Barrett 1980).

In Figure 4 we also show the $H_2O$ masers (Haschick *et al.* 1980; Henkel, Haschick, and Güsten 1986), near-IR sources (Strom, Vrba, and Strom 1976), and HH objects (von Hippel, Burnell, and Williams 1988) in the region. A remarkable result emerges from the comparison between the location of the HH objects and that of the H I blueshifted lobes: both in HH 7–11 and in HH 12, the HH objects appear to trace an edge of the blueshifted lobe. This result may imply that the HH objects, at least in these systems, do not necessarily trace a collimated, jetlike outflow (in this case one would expect the HH objects to be centered in the lobe), but the walls of the cavities created by the interaction of the stellar wind with the ambient medium (Cantó 1980; Cantó and Rodríguez 1980). It is along the walls of these cavities that the stellar wind will be stopped and shocked gas is expected to exist. A similar explanation has been proposed by Rodríguez *et al.* (1989*a*) for a chain of HH objects along the edge of the blueshifted lobe in L1551. It is not clear why only one side of the lobe is traced by the HH objects, but variable extinction in the ambient cloud could account for this effect. In the frame of this interpretation, the $HCO^+$ condensations observed in association with HH 7–11 by Rudolph and Welch (1988) would not be individual shocked ambient cloudlets, but corrugations along the walls of the wind-filled cavity. Molecular observations that could resolve the cavity walls, such as those of Uchida *et al.* (1987) and Moriarty-Schieven and Snell (1988) for L1551, are needed to test this hypothesis.

In contrast with the map from the redshifted channel that only shows two regions of emission, the map from the blueshifted channel shows, in addition to the features associated with HH 7–11 and HH 12, seven additional regions of emission and one of absorption (see Fig. 2 and Table 2). We believe that some of them could be regions of monopolar, blueshifted outflow. This suggestion is based on the fact that of the nine blueshifted H I emission regions, five are associated with radio sources (see Table 2). This association between blueshifted H I and continuum includes the blueshifted lobes of the HH 7–11 and HH 12 bipolar outflows. At present it is not clear why, in the case of the outflows associated with HH 7–11 and HH 12, we see radio continuum in association only with the blueshifted lobes. Obviously, the association of blueshifted H I with continuum sources favors the argument that these radio sources are associated with the HH 7–11 cloud and are not just background objects. In the Taurus complex, Heyer *et al.* (1987) found a preponderance of monopolar (in that case redshifted)

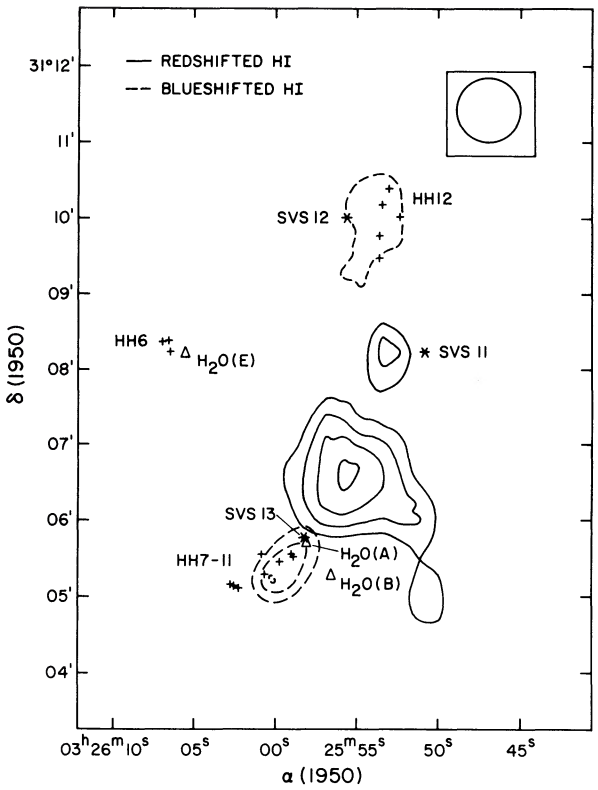


FIG. 4.—Redshifted H I (*solid line*: 18.3 to 38.9 km s$^{-1}$ velocity interval) and blueshifted H I (*dashed line*: −22.9 to −2.3 km s$^{-1}$ velocity interval) associated with HH 7–11 and HH 12. Contours are 3, 4, 5, and 6 mJy beam$^{-1}$. We also show the HH objects (*crosses*), near-IR sources (*asterisks*), and $H_2O$ masers (*triangles*) in the region.

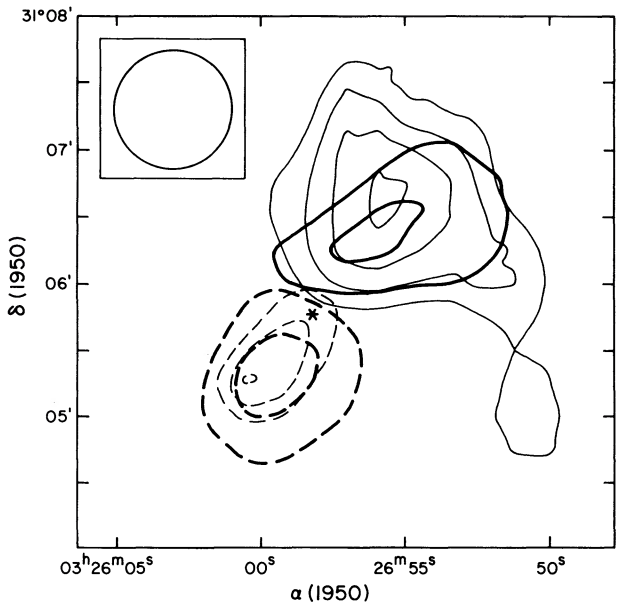


FIG. 5.—Redshifted (*heavy solid contours*) and blueshifted (*heavy dashed contours*) H I associated with HH 7–11 at ±41.2 km s$^{-1}$ with respect to the ambient cloud radial velocity. Contours are 3 and 4 times the 1 σ value 0.7 mJy beam$^{-1}$. In this figure we show also the redshifted (*thin solid contours*) and blueshifted (*thin dashed contours*) H I at ±20.6 km s$^{-1}$. Contours are 3, 4, 5, and 6 mJy beam$^{-1}$. The asterisk marks the position of SVS 13.

outflows. An alternative explanation is that we are observing line-of-sight blueshifted H I, perhaps associated with the large shell observed in the Galactic anticenter region (Kulkarni, Dickey, and Heiles 1985). The HH 7–11 region has Galactic coordinates $l = 158°.3$ and $b = -20°.6$ and appears projected close to the H I shell detected by Kulkarni *et al.* (1985).

For the total fluxes of the lobes associated with HH 7–11 and HH 12 we have estimated the outflow parameters, which are given in Table 3. Since we do not have detailed velocity information of the H I outflow, we derived the parameters assuming that the gas has a velocity of 20.6 km s$^{-1}$, the radial velocity shift of the channels with respect to the ambient cloud.

Finally, we point out that, at least in the case of L1551 (van der Werf *et al.* 1989) and HH 7–11 (this paper), the H I line can be used successfully to obtain information on the high-velocity gas of the bipolar outflows.

### *d*) H I *Line Emission at* ±41.2 km s$^{-1}$

We also detected the bipolar outflow associated with HH 7–11 in the 41.2 km s$^{-1}$ channel data. In Figure 5 we show this emission. The bipolar morphology of this high-velocity gas is similar to that seen in the 20.6 km s$^{-1}$ data. The total flux of the redshifted lobe is ∼10 mJy, while that of the blueshifted lobe is ∼5 mJy. We failed to detect emission in the higher velocity channels even after averaging over several velocity ranges.

## IV. DISCUSSION OF THE HIGH-VELOCITY H I

Lizano *et al.* (1988), using the Arecibo telescope, detected H I emission over a velocity range of ±170 km s$^{-1}$. Our VLA data is less sensitive (Arecibo has ∼6 times the collecting area of the VLA) but has better angular resolution (the VLA in the D configuration has ∼4 times higher angular resolution than Arecibo) than that of Lizano *et al.* (1988). Because of the lower sensitivity we detected H I emission only over ±60 km s$^{-1}$. But taking advantage of the higher angular resolution we can conclude that the high-velocity H I emission is clearly bipolar and has a similar morphology and orientation to that exhibited by the lower velocity CO mapped by Edwards and Snell (1983) and Liseau, Sandell, and Knee (1988). The mapping of the extremely high velocity CO in HH 7–11 (Koo 1989; Bachiller and Cernicharo 1990) indicates that also this component has a bipolar morphology.

Is the H I gas mapped by the VLA a lower velocity component of the extremely high-velocity H I detected with Arecibo? We believe that this is the case based on the following discussion. Lizano *et al.* (1988) modeled the H I wings as arising from a decelerating, optically thin biconical outflow. The velocity of the outflow follows a power-law velocity of the form $v(r) = Ar^{-1/\beta}$, with $r$ being the distance to the central source, and $A$ and $\beta$ constants. Then, the angular size of the outflow is expected to decrease with increasing velocity, $r \propto |v|^{-\beta}$. In agreement with this expectation, the ±41.2 km

TABLE 3

BIPOLAR OUTFLOW PARAMETERS FROM H I DATA[a]

| Sources | Lobe | Total Flux (mJy) | Mass ($M_\odot$) | Momentum ($M_\odot$ km s$^{-1}$) | Kinetic Energy (ergs) |
|---|---|---|---|---|---|
| HH 7–11 .... | Red | 26 | 0.015 | 0.31 | $6 \times 10^{43}$ |
| HH 7–11 .... | Blue | 6 | 0.003 | 0.07 | $1 \times 10^{43}$ |
| HH 12 ..... | Red | 5 | 0.003 | 0.06 | $1 \times 10^{43}$ |
| HH 12 ..... | Red | 10 | 0.006 | 0.12 | $2 \times 10^{43}$ |

[a] From the ±20.6 km s$^{-1}$ channels.

$s^{-1}$ maps show that the redshifted lobe is significantly more compact than the redshifted lobe seen in the $\pm 20.6$ km $s^{-1}$ maps (see Fig. 5). The centroid of the 20.6 km $s^{-1}$ redshifted lobe emission is at 62″ to the NW of SVS 13, while the centroid of the 41.2 km $s^{-1}$ redshifted lobe emission is at 43″ to the NW of SVS 13. We did not detect shifts between the centroids of the 20.6 km $s^{-1}$ and 41.2 km $s^{-1}$ blueshifted lobes; both peak at ~33″ to the SE of SVS 13. It is unclear at present if this implies that deceleration is not present in the blueshifted gas or if we lacked the angular resolution to detect it. From his high-velocity CO data, Bachiller and Cernicharo (1990) propose that deceleration is present in both lobes. From the position shift of the redshifted lobes we derive $\beta \simeq 0.6$. In addition, the Lizano *et al.* (1988) model predicts that the antenna temperature in the line wing emission will follow a power-law dependence of the form $T_A \propto |v|^{-(2+\beta)}$. After taking into account that the Arecibo sensitivity is 8.0 K $Jy^{-1}$, we find that a power-law fit for the flux density in the line wing emission (for the case $\beta = 0.6$) given by

$$\left(\frac{S_L}{\text{mJy}}\right) = 6.5\left(\frac{|v|}{41.2 \text{ km s}^{-1}}\right)^{-2.6}, \quad (4)$$

can account reasonably for the flux densities observed in Arecibo and the VLA for the redshifted gas, the one for which Lizano *et al.* (1988) have more reliable data (the blueshifted component of their spectra is contaminated by line-of-sight gas). Equation (4) gives, within 50%, the flux densities observed in the redshifted gas at 100.0 km $s^{-1}$ ($\simeq 1$ mJy; Arecibo), at 41.2 km $s^{-1}$ ($\simeq 10$ mJy; VLA), and at 20.6 km $s^{-1}$ ($\simeq 26$ mJy; VLA). We then believe that the H I mapped with the VLA is the decelerated, lower velocity extension of the extremely high velocity atomic gas detected by Lizano *et al.* with Arecibo. Furthermore, a decelerating, optically thin outflow accounts reasonably for the observations of the redshifted gas. Nevertheless, we have to note that the H I observed with the VLA could be H I in the stellar wind, dissociated $H_2$ from the ambient cloud, or a combination of both. As a result of the relatively low velocity of the observed material we cannot distinguish between these possibilities.

## V. CONCLUSIONS

We observed with the VLA at 21 cm the continuum and H I emission from the HH 7–11 region. Our main conclusions can be summarized as follows.

1. In the continuum we detected 58 sources in the region, most of them background objects. Nevertheless, several of the radio continuum sources are almost certainly associated with the HH 7–11 region, and their nature is discussed.

2. At the velocity of the ambient cloud, we detected H I emission regions around SVS 3 and BD +30°549, the illuminating stars of NGC 1333, the reflection nebula to the northeast of HH 7–11. We suggest that these zones are photodissociated H I regions.

3. The H I emission at $\pm 20$ km $s^{-1}$ maps two apparently independent bipolar outflows associated with HH 7–11 and with HH 12.

4. At higher velocities ($\pm 40$ km $s^{-1}$ with respect to the radial velocity of the ambient cloud), we can still detect the high-velocity bipolar H I emission associated with HH 7–11. The 40 km $s^{-1}$ redshifted H I emission is more compact than the 20 km $s^{-1}$ redshifted H I emission, as expected for a decelerating outflow.

We thank A. Dalgarno and D. Hollenbach for helpful comments. We acknowledge the Astronomical Data Center at the NASA Goddard Space Flight Center for providing the Red POSS digitized image of the HH 7–11 region. L. F. R. and J. C. acknowledge support from DGAPA-UNAM grant IN010589.

## APPENDIX

## THE H I REGIONS AROUND BD +30°549 AND SVS 3

In Figure 3 we showed the map of the H I emission around BD +30°549 and SVS 3. This emission is occurring at the velocity of the cloud ($v_{\text{LSR}} = 8.0$ km $s^{-1}$). The natural weighting maps have an angular resolution of ~53″, and these sources appear unresolved. To investigate further the nature of these H I components, we made line maps with uniform weighting, obtaining higher angular resolution (35″) but lower sensitivity. The H I emission associated with SVS 3 is clearly detected even at this lower sensitivity and a spatial cut in right ascension along its peak is shown in Figure 6. The beam is also shown in this figure, and we can appreciate that the source is resolved. From these data, we estimate a deconvolved angular diameter of 40″ ± 10″ for the H I region. From equation (2) and a total H I flux of $S_\nu = 30$ mJy, we derive an average brightness temperature of $T_B \simeq 16$ K ($\Delta v_i/\Delta v_l$). Given our lack of velocity resolution ($\Delta v_i \simeq 20$ km $s^{-1}$), we did not resolve the line width. Nevertheless, from what is known of other photodissociated H I regions (Dewdney and Roger 1982), we adopt a line width of $\Delta v_l \simeq 4$ km $s^{-1}$ and then derive $T_B \simeq 80$ K. Since the excitation temperature of H I in a photodissociated region is of order ~500–1000 K (Tielens and Hollenbach 1985), we will assume that the H I emission is optically thin.

We can then use equation (3) to derive an H I mass of 0.017 $M_\odot$. At a distance of 350 pc, the source has a radius, $R \simeq 0.03$ pc and a density of $n_{\text{H I}} \simeq 6 \times 10^3$. The radius of the H I region will then have a column density of $N_{\text{H I}} \simeq 6 \times 10^{20}$ $\text{cm}^{-2}$. Are these parameters in agreement with the $H_2$ dissociation expected from a B5 star like SVS 3? To discuss this question quantitatively, we made numerical models of the photodissociated region around B-type stars (Escalante *et al.* 1990). These models have spherical symmetry, uniform density and gas temperature, and use the same parameters of the plane-parallel models of Sternberg and Dalgarno (1989). The results of the numerical models can be fitted to an expression of the form

$$\left(\frac{\dot{N}_{\text{UV}}}{10^{30} \text{ s}^{-1} \text{ Hz}^{-1}}\right) = 0.73\left(\frac{M_{\text{H I}}}{0.01\ M_\odot}\right)^2\left(\frac{R}{0.01 \text{ pc}}\right)^{-3} \exp\left[4.70\left(\frac{M_{\text{H I}}}{0.01\ M_\odot}\right)\left(\frac{R}{0.01 \text{ pc}}\right)^{-2}\right], \quad (A1)$$

where $\dot{N}_{\text{UV}}$ is the photon rate per Hz produced by the central star at 1000 Å. In terms of observable quantities, the above equation can be set as

$$\left(\frac{\dot{N}_{\text{UV}}}{10^{30} \text{ s}^{-1} \text{ Hz}^{-1}}\right) = 2.72 \times 10^{-2}\left(\frac{S_\nu}{\text{mJy}}\right)^2\left(\frac{\Delta v}{\text{km s}^{-1}}\right)^2\left(\frac{D}{\text{kpc}}\right)\left(\frac{\theta_D}{\text{arcsec}}\right)^{-3} \exp\left[1.84\left(\frac{S_\nu}{\text{mJy}}\right)\left(\frac{\Delta v}{\text{km s}^{-1}}\right)\left(\frac{\theta_D}{\text{arcsec}}\right)^{-2}\right]. \quad (A2)$$

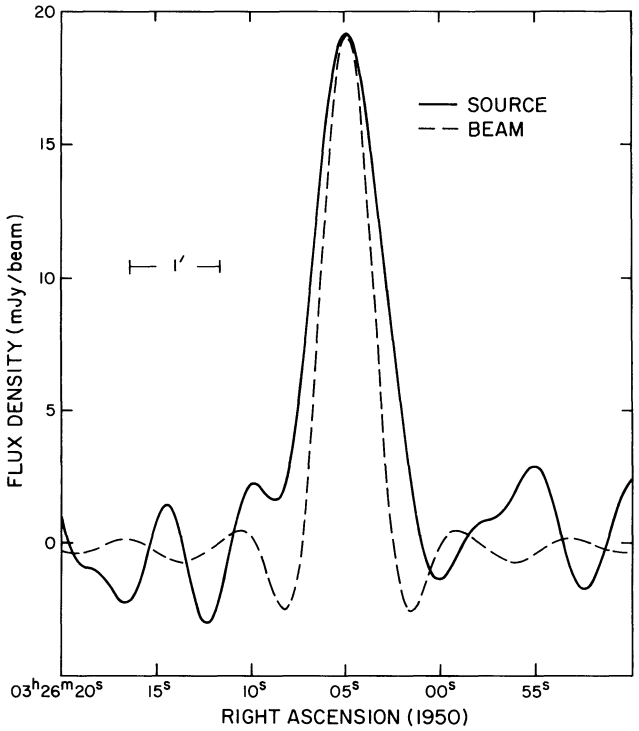


FIG. 6.—Spatial cut along the peak of the H I emission associated with SVS 3 (*solid line*) and along the peak of the beam (*dashed lines*). The cuts were made at a fixed declination. The source emission appears to be resolved spatially.

In this equation $\Delta v$ is the instrumental width since the line is not resolved in velocity, $D$ is the distance to the source, and $\theta_D$ is the angular diameter of the source. We point out that the determination of $\dot{N}_{UV}$ is very sensitive to the value of $\theta_D$. Using the parameters derived above, we obtain $\dot{N}_{UV} = 10^{29.3\pm1.2}$ s$^{-1}$ Hz$^{-1}$, with the large error being mainly due to the uncertainty in $\theta_D$. This range of values includes, at its high end, the value of $\dot{N}_{UV} = 2.4 \times 10^{30}$ s$^{-1}$ Hz$^{-1}$ expected for a B5 ZAMS star. We then conclude that the observational results are, within the uncertainty, consistent with the modeling for a photodissociated region and that new observations where the source emission is resolved angularly and in velocity are required for a more adequate comparison.

## REFERENCES


Bachiller, R., and Cernicharo J. 1990, *Astr. Ap.*, in press.
Cantó, J., and Rodríguez, L. F. 1980, *Ap. J.*, **239**, 983.
Cohen, M., and Schwartz, R. D. 1983, *Ap. J.*, **265**, 877.
Condon, J. J. 1984, *Ap. J.*, **287**, 461.
Curiel, S., Rodríguez, L. F., Cantó. J., Bohigas, J., Roth, M., and Torrelles, J. M. 1989, *Ap. Letters Comm.*, **27**, 299.
Dewdney, P. E., and Roger, R. S. 1982, *Ap. J.*, **255**, 564.
———. 1986, *Ap. J.*, **307**, 275.
Edwards, S., and Snell, R. L. 1983, *Ap. J.*, **270**, 605.
Escalante, V., Cantó, J., Rodríguez, L. F., and Lizano, S. 1990, in preparation.
Grossman, E. N., Masson, C. R., Sargent, A. I., Scoville, N. Z., Scott, S., and Woody, D. P. 1987, *Ap. J.*, **320**, 356.
Harvey, P. M., Wilking, B. A., and Joy, M. 1984, *Ap. J.*, **278**, 156.
Haschick, A. D., Moran, J. M., Rodríguez, L. F., Burke, B. F., Greenfield, P., and García-Barreto, J. A. 1980, *Ap. J.*, **237**, 26.
Henkel, C., Haschick, A. D., and Güsten, R. 1986, *Astr. Ap.*, **165**, 197.
Herbig, G. H., and Jones, B. F. 1983, *A.J.*, **88**, 1040.
Heyer, M. H., Snell, R. L., Goldsmith, P. F., and Myers, P. C. 1987, *Ap. J.*, **321**, 370.
Ho, P. T. P., and Barrett, 1980, *Ap. J.*, **237**, 38.
Koo, B. 1989, *Ap. J.*, **337**, 318.
Jennings, R. E., Cameron, D. H. M., Cudlip, W., and Hirst, C. J. 1987, *M.N.R.A.S.*, **226**, 461.
Klinglesmith, D. A., and Hollis, H. M. 1987, *Ap. J. Suppl.*, **64**, 127.
Kulkarni, S. R., Dickey, J. M., and Heiles, C. 1985, *Ap. J.*, **291**, 716.
Liseau, R., Sandell, G., and Knee, L. B. G. 1988, *Astr. Ap.*, **192**, 153.
Lizano, S., Heiles, C., Rodríguez, L. F., Koo, B., Shu, F. H., Hasegawa, T., Hayashi, S., and Mirabel, I. F. 1988, *Ap. J.*, **328**, 763.
Moriarty-Schieven, G. H., and Snell, R. L. 1988, *Ap. J.*, **332**, 364.
Natta, A., Giovanardi, C., Palla, F., and Evans, N. J. 1988, *Ap. J.*, **327**, 817.
Read, P. L. 1980, *M.N.R.A.S.*, **192**, 11.
Rodríguez, L. F., and Cantó, J. 1983, *Rev. Mexicana Astr. Ap.*, **8**, 163.
Rodríguez, L. F., Cantó, J., López, A., and Moreno, M. A. 1989*a*, *Rev. Mexicana Astr. Ap.*, **17**, 111.
Rodríguez, L. F., Myers, P. C., Cruz-González, I., and Terebey, S. 1989*b*, *Ap. J.*, **347**, 461.
Rudolph, A., and Welch, W. J. 1988, *Ap. J. (Letters)*, **326**, L31.
Sandell, G., Aspin, C., Duncan, W. D., Robson, E. I., and Dent, W. R. F. 1990, *Astr. Ap.*, **232**, 347.
Snell, R. L., and Bally, J. 1986, *Ap. J.*, **303**, 683.
Sternberg, A., and Dalgarno, A. 1989, *Ap. J.*, **338**, 197.
Strom, K. M., Strom, S. E., and Stocke, J. 1983, *Ap. J. (Letters)*, **271**, L23.
Strom, S. E., Vrba, F. J., and Strom, K. M. 1976, *A.J.*, **81**, 314.
Tielens, A. G. G. M., and Hollenbach, D. 1985, *Ap. J.*, **291**, 722.
Thompson, R. I. 1984, *Ap. J.*, **283**, 165.
Uchida, Y., Kaifu, N., Shibata, K., Hayashi, S. S., Hasegawa, T., and Hamatake, H. 1987, *Pub. Astr. Soc. Japan*, **39**, 907.
van der Werf, P. P., Dewdney, P. E., Goss, W. M., and vanden Bout, P. A. 1989, *Astr. Ap.*, **216**, 215.
von Hippel, T., Burnell, S. J. B., and Williams, P. M. 1989, *Astr. Ap. Suppl.*, **74**, 431.


JORGE CANTÓ, VLADIMIR ESCALANTE, LUIS F. RODRÍGUEZ, and SUSANA LIZANO: Instituto de Astronomía, UNAM, Apdo. Postal 70-264, 04510 México, D. F., Mexico

I. FELIX MIRABEL: Service d'Astrophysique, Institut de Recherche Fondamentale, CEA-CEN Saclay, 91191 Gif-sur-Yvette, France